Supporting Information

Photocatalytic H_2 evolution coupled with selective aromatic alcohol oxidation over nitrogen-vacancy-rich $Ti_3C_2T_x$/g-C_3N_4 junctions via interfacial N-Ti bonding

Wen-Jing Yi,[a] Xin Du,[a] Sha-Sha Yi,[b] Yanyan Liu,[c] Baojun Li,[b] Zhong-Yi Liu[a,*] and Xin-Zheng Yue[a,*]

[a]College of Chemistry, Zhengzhou University, Zhengzhou 450001, China.

[b]School of Materials Science and Engineering, Zhengzhou University, Zhengzhou 450001, China

[c]College of Science, Henan Agricultural University, Zhengzhou 450002, China

*Corresponding authors: liuzhongyi@zzu.edu.cn; yuexz@zzu.edu.cn

1. Experimental section

1.1 Chemicals and materials

Ti_3AlC_2 (98%) was bought from Shanghai Macklin Reagent. Hydrofluoric acid (HF, ≥40%), urea (99%), triethanolamine (TEOA), carbon tetrachloride (CCl_4) and sodium sulfate anhydrous (Na_2SO_4, 99%) were purchased from Fengchuan Chemical Reagent Technology Co., Ltd. Nafion solution (Dupont, 5 wt%), deuterium oxide (D_2O), furfuryl alcohol, furfural, 5-hydroxymethylfurfural, benzyl alcohol, and other several aromatic alcohols were all obtained from Aladdin Chemicals. All the chemicals were analytical reagents and used directly without further purification. Fluorine-doped tin oxide (F:SnO_2, FTO<15 Ω sq^{-1}) glass was acquired from Zhuhai Kaivo Optoelectronic Technology Co., Ltd. N_2/H_2 mixture gas (10 vol% of H_2) was acquired from Henan Yuanzheng Special Gas Co., Ltd. Deionized water (18.2 MΩ·cm) was used in all the preparations.

1.2 Synthesis of $Ti_3C_2T_x$ (TC) *and r-TC MXene*

$Ti_3C_2T_x$ MXenes were synthesized by a facile acid treatment approach using Ti_3AlC_2 as the precursor material. In a typical experiment, 1 g of Ti_3AlC_2 powers were mixed with 15 mL of HF and stirred at 30°C for 36 h. The obtained suspension was centrifuged at 3500 rpm for 10 min, rinsed thoroughly with deionized water until a pH value of 7 was achieved, and then dried at 60°C in a vacuum oven. The obtained $Ti_3C_2T_x$ powers were designated as TC MXenes. To obtain surface reduced TC MXene (labeled as r-TC), 0.5 g of TC MXenes were heated at 550°C for 2 h in an N_2/H_2 mixture gas (10 vol% of H_2).

1.3 Synthesis of 2D/2D TC/CN

Typically, 20 g of urea was dispersed in deionized water containing various amounts of TC MXenes (15, 20, 25, 35, and 45 mg), followed by ultrasonic treatment for 2 h under a N_2 atmosphere in an ice-water bath. Due to hydrogen bonding interactions between the terminal functional groups (-O/-F) of TC and the amine groups of urea, a uniform distribution of urea was achieved on the surface of TC. After drying in vacuum overnight and calcining at 550°C for 2 h under N_2/H_2 atmosphere, the photocatalysts were obtained and designated as TC(*m*%)/CN (*m* = 2.5, 3.5, 5.3, 7.5, and 9.1), where *m* represents the practical mass content of TC. The TC(5.3%)/CN sample in this study was labeled as TC/CN unless otherwise specified. Pristine g-C_3N_4 (CN) was obtained through the same procedure described above, excluding the utilization of TC. The CN-air was synthesized via direct pyrolysis of urea (20 g) at 550°C for 2 h in a muffle furnace. $Ti_3C_2T_x$&g-C_3N_4 (r-TC&CN) was synthesized by mixing 5.3 mg of r-TC and 94.7 mg of CN in 10 mL of deionized water, followed by sonication for 0.5 h.

1.4 Characterization

Morphologies and microstructures of as-prepared photocatalysts were characterized by field-emission scanning electron microscopy (FESEM, JEOL JSM 6700F), transmission electron microscopy (TEM, Tecnai G2 S-Twin F20 with 200 kV, FEI), and high-resolution TEM (HRTEM) images, and atomic force microscopy (AFM, SPM-8100FM, Shimadzu Co.). X-ray photoelectron spectroscopy (XPS) was conducted on a VG Scientific ESCALAB 250 spectrometer (Thermo) with Al Kα X-ray excitation. All XPS spectra were calibrated using the C 1s peak at a banding energy of 284.8 eV. The crystalline structures of catalysts were determined using power X-ray diffraction

(XRD) with a D/Max-2550 diffractometer (Rigaku), which operated at 50 kV and 200 mA, and utilized Cu Kα radiation (λ = 1.54056 Å). The range of 2θ angles examined was from 5 to 80°. Fourier-transform infrared (FTIR) spectroscopy was measured by a TENSOR II FTIR spectrometer (Bruker) with a wavenumber range of 4000-400 cm^{-1}. Thermogravimetric (TG, STA2500-0412-N, NETZSCH) analysis was performed in the temperature range of 50 to 800°C with a heating rate of 10°C min^{-1}. The specific surface area and the pore size distribution were respectively analyzed by Brunauer-Emmett-Teller (BET) method and Barrett-Joyner-Halenda (BJH) formula on the basis of nitrogen adsorption-desorption isotherms measured on the ASAP 2460-4MP sorptometer (Micromeritics) at –196°C. Before measurements, all samples were degassed at 150°C for 4 h. Ultraviolet-visible diffusion reflectance spectra (UV-vis DRS) were acquired using the UH-4150 ultraviolet/visible/near-infrared spectrophotometer (Hitachi), which was equipped with an integrated sphere in the wavelength range of 300 to 800 nm using $BaSO_4$ as a reference. The steady-state photoluminescence (PL) emission spectra were measured using FluoroMax-4 spectrofluorometers (HORIBA) with an excitation wavelength of 320 nm. Time-resolved PL (TRPL) decay spectra were obtained on a FLS 980 spectrofluorometer (Edinburgh) with an emission wavelength of 440 nm. Gas chromatography-mass spectrometry (GC-MS) was conducted on GCMS-QP2020 NX (Shimadzu Co., Japan) with He as carrier gas. At room temperature, electron paramagnetic resonance (EPR) was tested using an EMXplus-9.5/12 spectrometer (Bruker) at 9.44 GHz. For *in-situ* EPR measurement, 5 mg of photocatalysts were dispersed in a 10 mL of furfuryl alcohol (FOL) aqueous solution (2 mM) containing the spin-trapping agent 5,5-dimethyl-1-pyrroline (DMPO). The suspension was introduced into a glass capillary, which was subsequently sealed in a glass tube under an Ar

atmosphere. Finally, EPR measurements were carried out under 300 W Xe lamp irradiation.

The femtosecond pump-probe transient absorption (fs-TA) measurements were performed using a regeneratively amplified Ti:sapphire laser system (Coherent; 800 nm, 100 fs, 7 mJ/pulse, and 1 kHz repetition rate) as the laser source and a HELIOS spectrometer (Ultrafast Systems LLC) as the spectrometer. The white-light continuum (820-1250 nm) probe pulse was generated by focusing the 800 nm beam (split from a regenerative amplifier with a tiny portion) onto sapphire. The time delay (0-8 ns) between the pump and probe pulses was varied by a motorized optical delay line. A mechanical chopper operating at 500 Hz was used to modulate the pump pulses such that the fs-TA spectra with and without the pump pulses could be recorded alternately. The samples dispersed in water were contained in 2-mm quartz cuvettes under a continuous magnetic stirring condition, ensuring that the photoexcited volume of the sample was kept fresh during the fs-TA measurements.

1.5 Photo- and electrochemical tests

The photo- and electrochemical measurements were conducted on an electrochemical workstation (RST5810F, Inc., Zhengzhou) with a standard three-electrode system consisting of working electrodes (FTO glasses coated with samples), counter electrode (Pt wire), and reference electrode (saturated Ag/AgCl electrode). An aqueous solution of 0.5 M Na_2SO_4 was used as the electrolyte, and a 300 W Xe lamp (CEL-HXF 300, 100 mW cm^{-2}) equipped with an AM 1.5G filter was utilized as the simulated solar light source. For the preparation of the working electrode, a suspension was obtained by mixing 5 mg of as-prepared samples with 350 μL of deionized water, 100 μL of ethanol and 50 μL of Nafion solution. The resulting mixture (50 μL) was uniformly dip-coated onto a piece of FTO glass (1 cm × 3 cm), followed by heating at 80°C for 2 h in a vacuum

drying oven. Current-time (*i-t*) curves were measured at -0.3 V *vs*. Ag/AgCl under intermittent light irradiation. Electrochemical impedance spectroscopy (EIS) Nyquist plots were measured under light irradiation at a potential of 0 V *vs*. Ag/AgCl, with a frequency range from 100 kHz to 0.01 Hz and an AC amplitude of 5 mV. Open circuit photovoltage (OCP) decay profiles were measured following cessation of light irradiation to analyze charge recombination behaviors. Linear sweep voltammetry (LSV) curves were recorded with a scan rate of 10 mV s^{-1}. Mott-Schottky (M-S) measurements were performed in the photovoltage range from -1.2 to 0.2 V *vs*. Ag/AgCl with different frequencies and an amplitude of 10 mV.

1.6 Photocatalytic activity tests

The photocatalytic H_2 evolution coupled with biomass conversion was conducted in a 300 mL quartz glass top-irradiation reaction cell at 5°C using an online trace gas analysis system (PerfectLight, Beijing, Labsolar-6A). Typically, 25 mg of photocatalysts were dispersed in 100 mL of furfuryl alcohol (FOL) aqueous solution (2 mM) containing the required amount of H_2PtCl_6 (3 wt% Pt). Before the reaction, the suspension was sonicated for 10 min and was subsequently purged with Ar gas to effectively eliminate any dissolved oxygen. To trigger the photocatalytic reaction, a 300 W Xe lamp (Perfect Light, Beijing, PLS-SXE300/300UV) was placed on top of the reaction cell as a full-spectrum light source and the suspension was stirred to ensure uniform illumination. The produced H_2 at different reaction times was monitored using an online gas chromatograph (GC-2014C, Shimadzu Co., Japan, 5 Å molecular sieve column with Ar as the carrier gas) equipped with a thermal conductivity detector (TCD). The liquid products were analyzed by high performance liquid chromatography (HPLC, Waters, C18 column) analysis equipped with UV-vis detector. In the

recycling stability test, photocatalytic activity was evaluated over 6 cycles of 36 h. Similarly, photocatalytic conversion of alternative aromatic alcohols coupled with H_2 evolution was conducted, except that the reaction substrate was substituted.

To explore the reaction mechanism of FOL conversion, a series of experiments on active species and carrier trapping were conducted. The quenching agents employed in this experiment included triethanolamine (TEOA, a hole scavenger), carbon tetrachloride (CCl_4, an electron scavenger), isopropanol (IPA, a hydroxyl radical scavenger), and 5,5-dimethyl-1-pyrroline (DMPO, a radical scavenger). We calculated the FOL conversion as well as the yield and selectivity of furfural (FAL) as follows:

$$\text{Conversion (\%)} = [(C_0 - C_{FOL})/C_0] \times 100\% \quad (1)$$

$$\text{Yield (\%)} = (C_{FAL}/C_0) \times 100\% \quad (2)$$

$$\text{Selectivity (\%)} = [C_{FAL}/(C_0 - C_{FOL})] \times 100\% \quad (3)$$

where C_0, C_{FOL}, and C_{FAL} are the concentrations of initial FOL, residual FOL, and produced FAL after a certain reaction time, respectively.

The utilization rate (R_U) is defined as the ratio of photogenerated electrons participating in H_2 evolution to holes participating in FAL production, which can be calculated as follows:

$$R_U = (\text{Numbers of evolved } H_2)/(\text{Numbers of DFF}) \times 100\% \quad (4)$$

The apparent quantum efficiency (AQE) of H_2 evolution was measured using monochromatic light sources of 400, 420, 450, 500 and 550 nm under the above-mentioned reaction conditions.

1.7 Theoretical calculations

Density function theory (DFT) calculations were conducted using the Vienna Ab initio Simulation Package (VASP) program. The generalized gradient approximation (GGA) with Perdew-Burke-Ernzerhof (PBE) functional was used for structure optimization. The cutoff energy of atomic wave functions was 400 eV. The Monkhorst-Pack k-point meshes were 3×3×1 and 3×3×1 for TC and CN, respectively. During the optimizations, the force on each atom and the total energy convergence criterion were set to be 0.05 eV/Å and 10^{-4} eV/atom, respectively.

The Gibbs free energy of intermediates for FOL oxidation to FAL was calculated by $\Delta G = \Delta E + \Delta E_{ZPE} - T\Delta S$, in which ΔE, ΔE_{ZPE} and ΔS represent the electronic energy, zero-point energy, and entropy difference between products and reactants, respectively. Zero-point energies of isolated and absorbed molecules were calculated by frequency analysis. The entropy of all molecules was obtained from the database of the National Institute of Standards and Technology (NIST).

Supplementary Figures

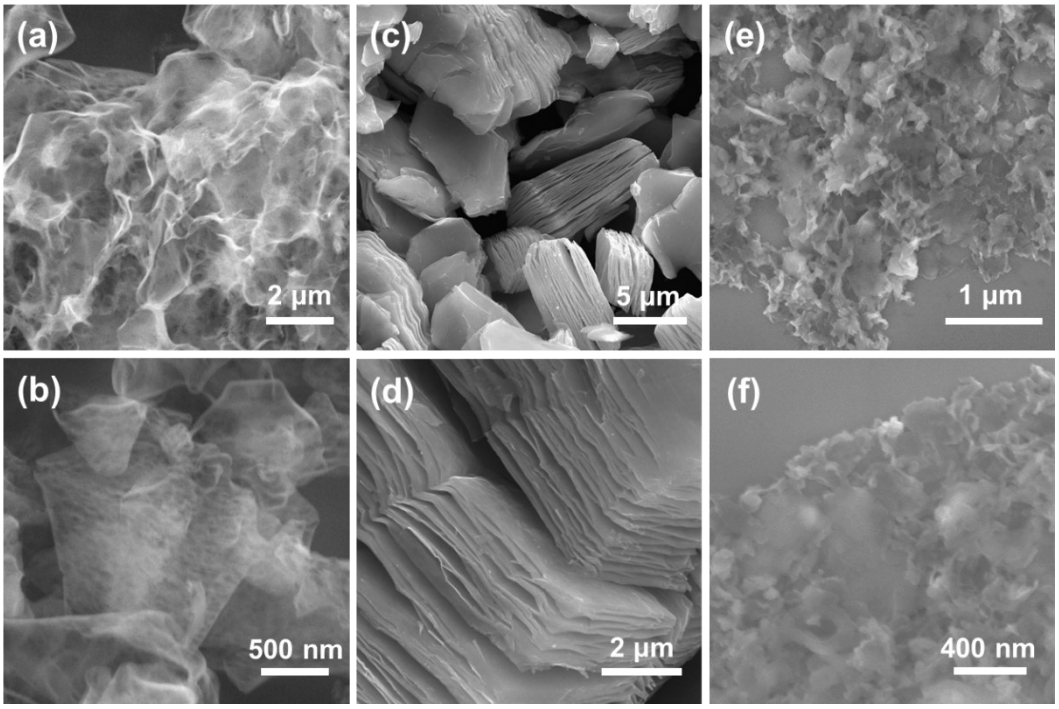

Figure S1. FESEM images of a,b) CN, c,d) TC, and e,f) TC/CN.

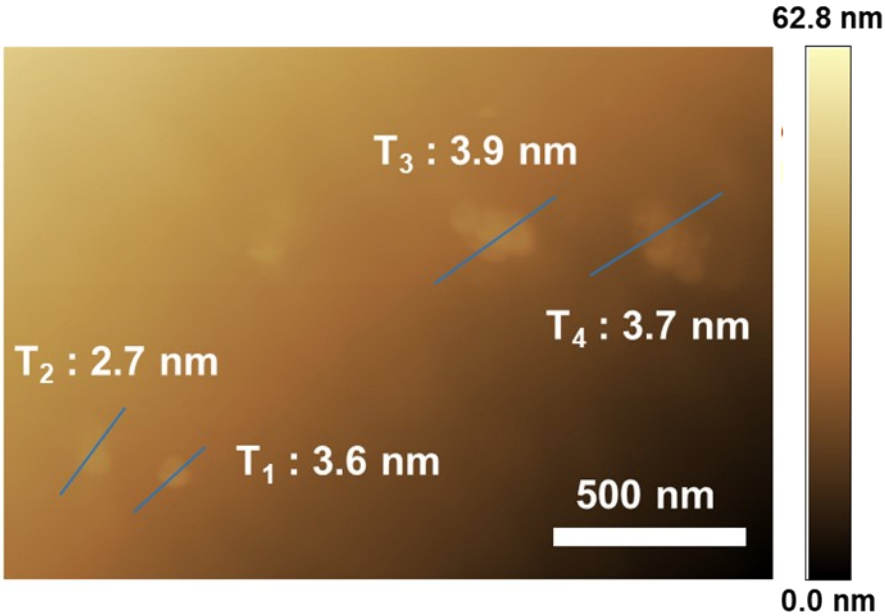

Figure S2 AFM image of TC/CN. Here, T_x (x = 1-4) represents the thickness of nanosheets.

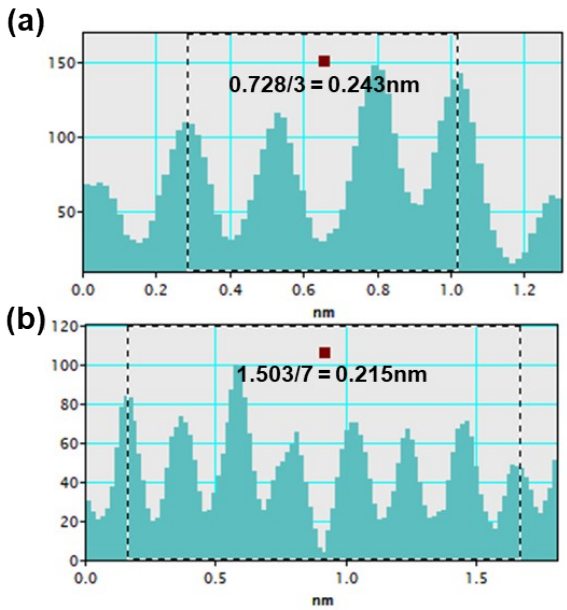

Figure S3. a,b) HRTEM-based line-intensity profiles of crystal fringes of TC in TC/CN.

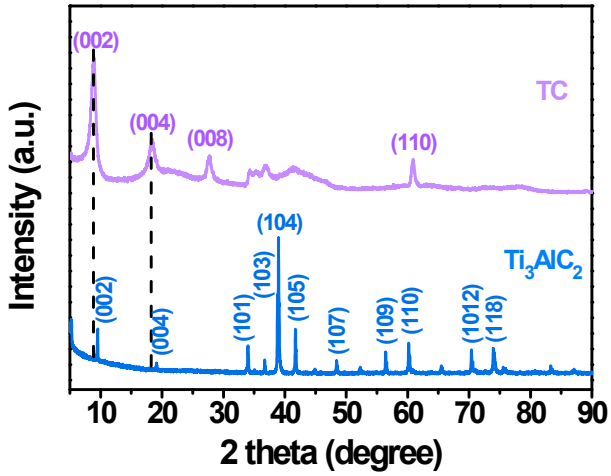

Figure S4. XRD patterns of TC and Ti_3AlC_2.

As shown in Figure S4, the dominant (104) peak of Ti_3AlC_2 at 39.2° disappeared, while the characteristic (002) and (004) peaks exhibited a shift towards lower degree. This indicates the successful removal of Al layers through HF etching and the transformation of pristine Ti_3AlC_2 into TC.[1]

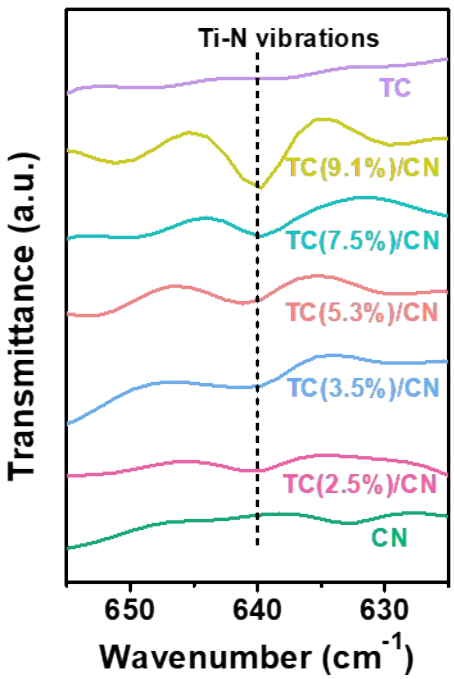

Figure S5. FTIR spectra of CN, TC, and TC(*m*%)/CN (*m* = 2.5, 3.5, 5.3, 7.5, and 9.1) in wavenumber of 625 to 655 cm^{-1}.

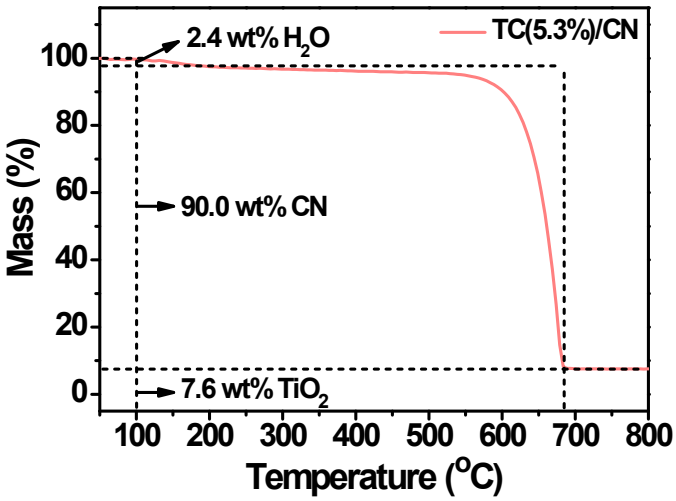

Figure S6. TG curve of TC(5.3%)/CN.

To calculate the TC content in hybrids, we take TC(5.3%)/CN as an example. The TG measurements were conducted under air atmosphere at temperatures ranging from 50 to 800°C. As shown in Figure S6, when the temperature is increased to 700°C, the g-C_3N_4 component can be

eliminated. At around 700°C, only 7.6 wt% of TiO_2 remains, which is equivalent to 18.4 wt% of the TC component. This is because that TC will completely oxidize to TiO_2 once the temperature reaches 800°C. Based on a constant amount of Ti atoms, the mass fraction of TC can be calculated as x% using Equation 5:

$$\frac{7.6\%}{3 \times \text{Molecular weight } (TiO_2)} = \frac{x\%}{\text{Molecular weight (TC)}} \quad \text{.....} \quad \text{.....(5)}$$

The molecular weight of TiO_2 and TC are 79.8 and 168.0 g mol^{-1}, respectively. Therefore,

$$\frac{7.6\%}{3 \times 79.8 \text{ g mol}^{-1}} = \frac{x\%}{168.0 \text{ g mol}^{-1}}$$

Consequently, the calculated mass fraction of TC in a hybrid material of TC(5.3%)/CN is approximately 5.33%.

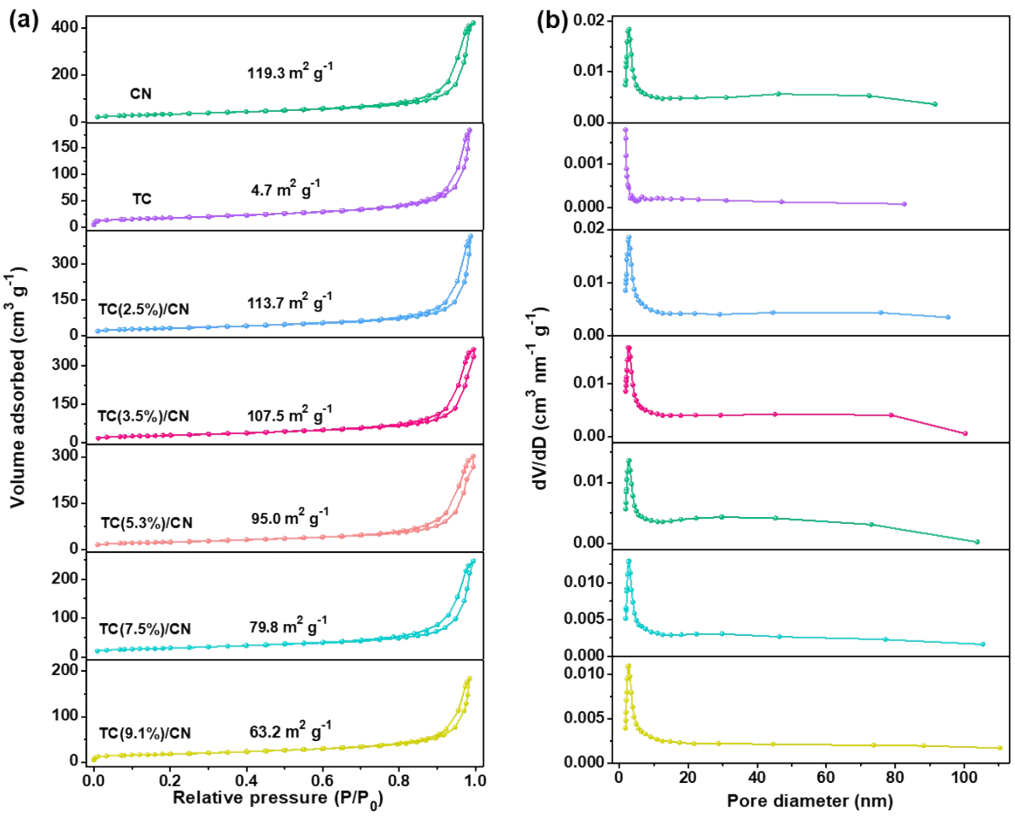

Figure S7. a) Nitrogen adsorption-desorption isotherms and b) the corresponding pore size distribution curves of CN, TC, and TC(*m*%)/CN.

To investigate the surface structure and specific surface area of the catalyst, N_2 adsorption-desorption isotherms were measured (Figure S7). All samples exhibited typical type-IV isotherms with H3 hysteresis behavior, indicating a mesoporous structure. TC and CN show specific surface areas of 4.7, and 119.3 m^2 g^{-1}, respectively. As for TC(*m*%)/CN, the surface area gradually decreases with an increase in TC content.

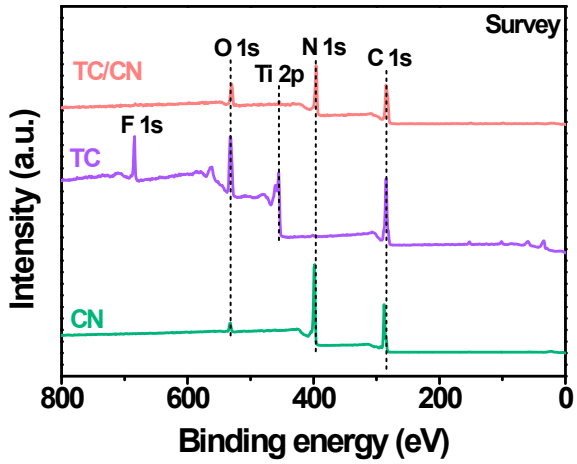

Figure S8. Survey XPS spectra of CN, TC, and TC/CN.

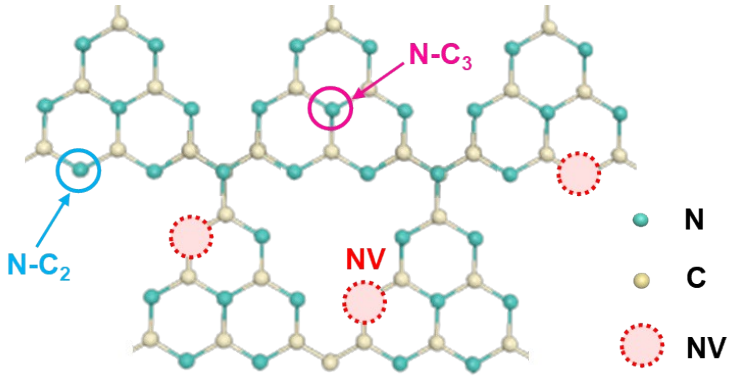

Figure S9. Atomic structural model of CN with NVs.

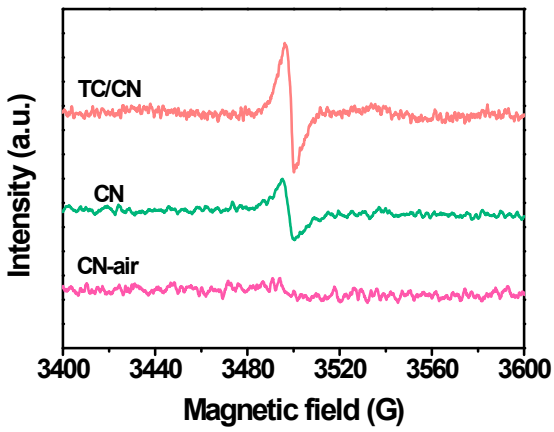

Figure S10. EPR spectra of CN-air, CN, and TC/CN.

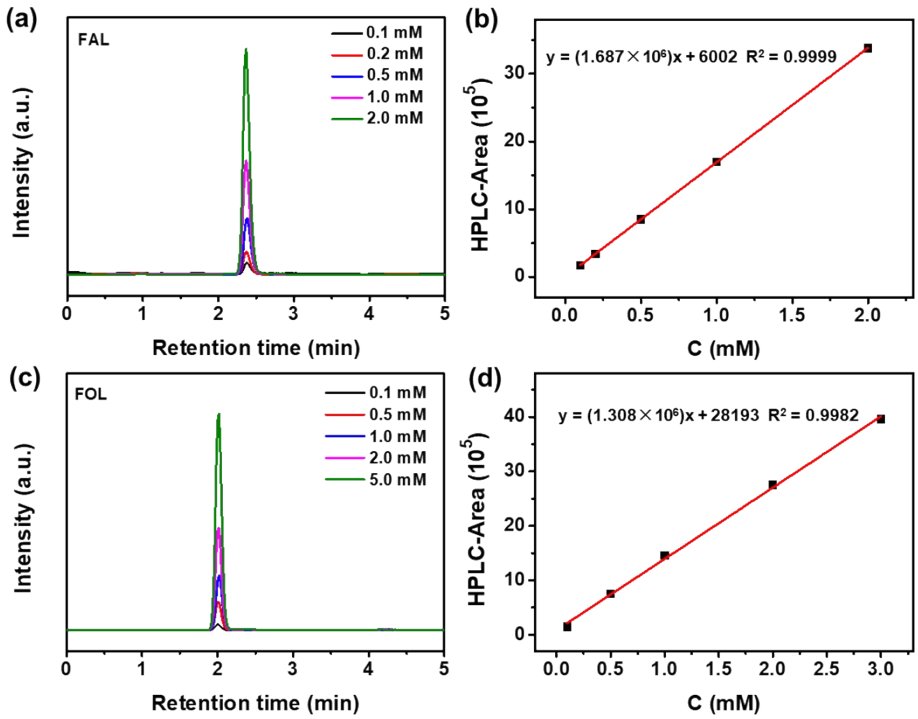

Figure S11. HPLC analysis of a) FAL and c) FOL with different concentrations. Calibrated linear relationship between peak area and the concentration of b) FAL and d) FOL.

A linear fit equation of $y = (1.687\times10^6)\,x + 6002$ can be obtained by analyzing the peak area at different FAL concentrations (Figure S11a), as shown in Figure S11b, with a fitting coefficient of $R^2 = 0.9999$. Based on the peak area calculated at different FOL concentrations (Figure S11c), a linear fit of $y = (1.308\times10^6)\,x + 28193$ we obtained from Figure S11d, with a fitting coefficient is R^2 =

0.9982.

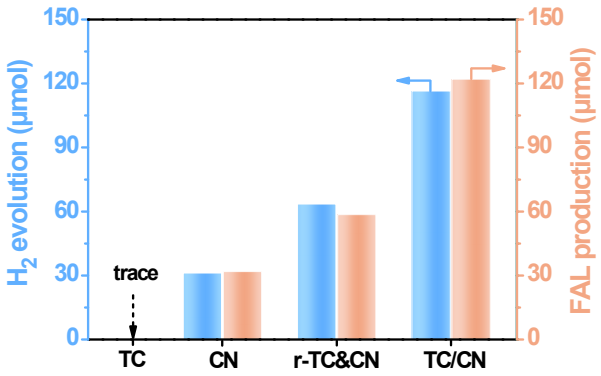

Figure S12. Photocatalytic activity of H_2 evolution coupled with FAL production over different samples.

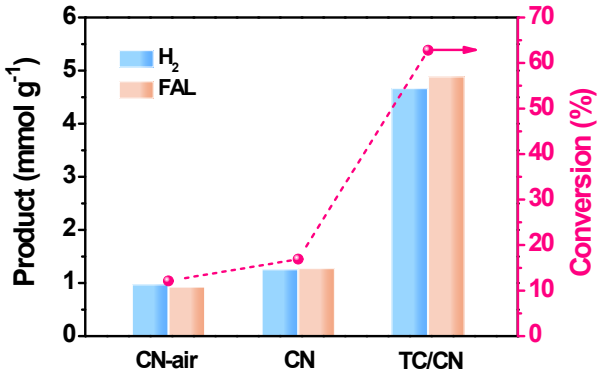

Figure S13. Photocatalytic oxidation of FOL to FAL and H_2 evolution activities of CN-air, CN, and TC/CN.

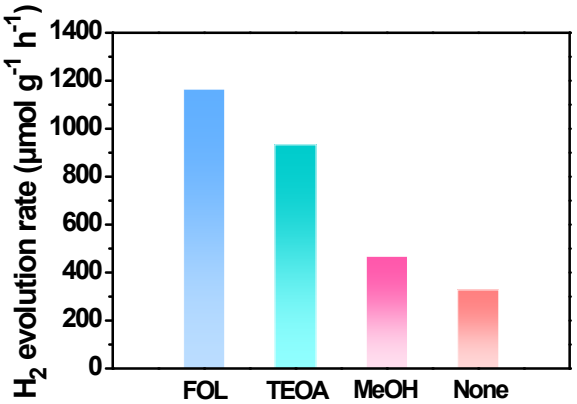

Figure S14. Photocatalytic H_2 evolution rates of TC/CN under various kinds of hole scavenger conditions.

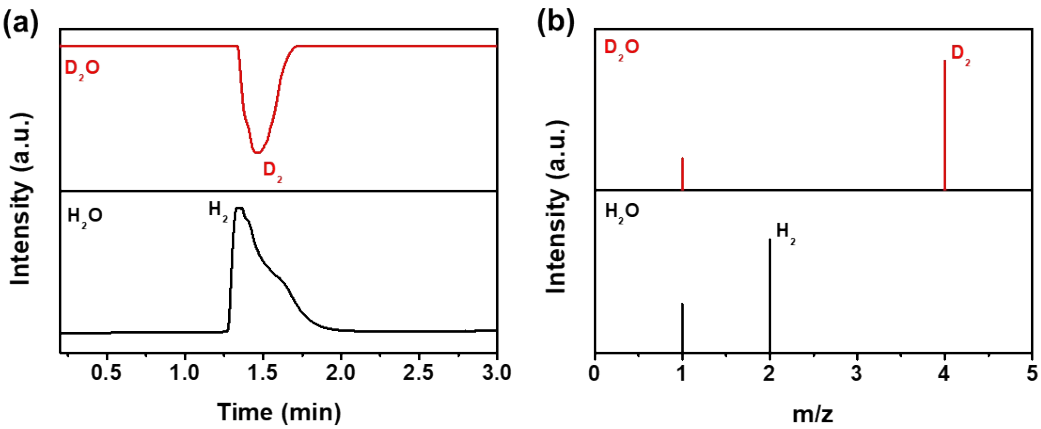

Figure S15. (a) GC and (b) MS spectra of TC/CN measured in H_2O and D_2O reaction solutions, respectively. The carrier gas for GC was He.

To further investigate the origin of H_2, we have conducted a hydrogen isotope test using D_2O as a substitute for H_2O in the reaction solution. As shown in Figure S15, D_2 (m/z = 4) was detected in mass spectrometry (MS) when the reaction was conducted in D_2O, whereas H_2 (m/z = 2) was the predominant product when H_2O served as the hydrogen source.

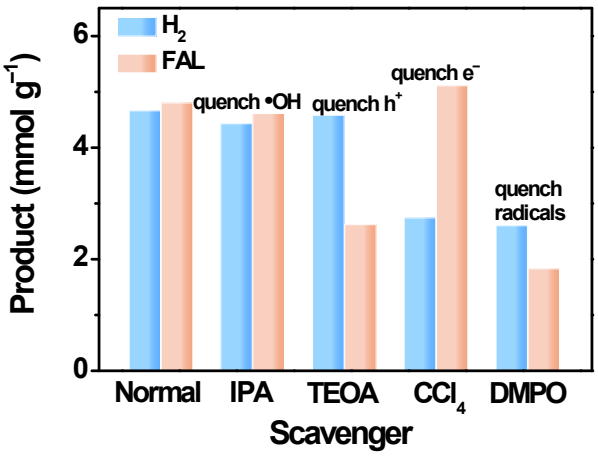

Figure S16. Control experiments with different scavengers over TC/CN.

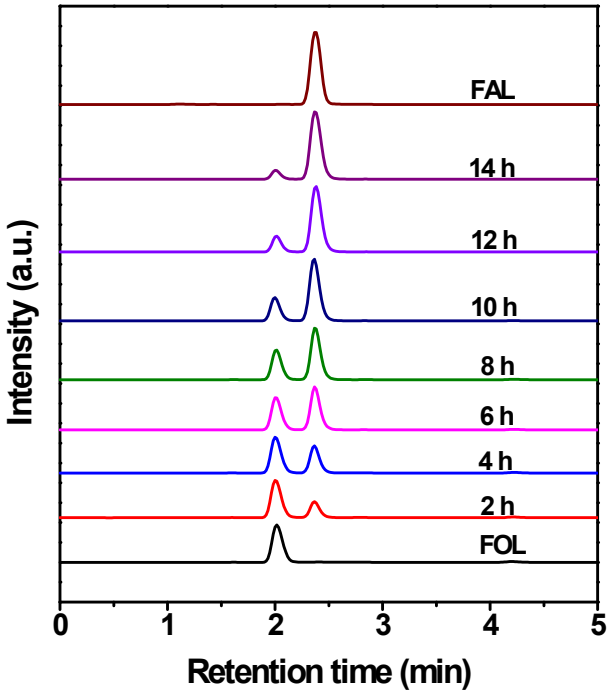

Figure S17. Time-dependent HPLC analysis of reaction solutions over TC/CN. Light source: simulated solar light irradiation. Reaction solution: 100 mL of deionized water containing 0.4 mmol of FOL. Catalyst: 25 mg.

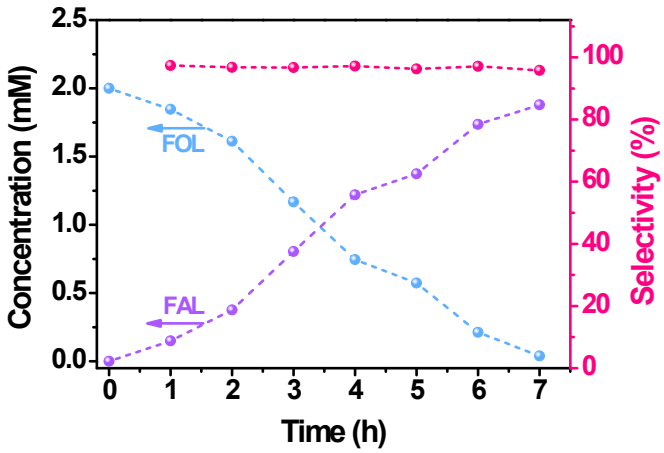

Figure S18. Evolution kinetics and selectivity of FAL as well as the corresponding consumption kinetics of FOL by HPLC analysis. Light source: simulated solar light irradiation. Reaction solution: 100 mL of deionized water containing 0.2 mmol of FOL. Catalyst: 25 mg.

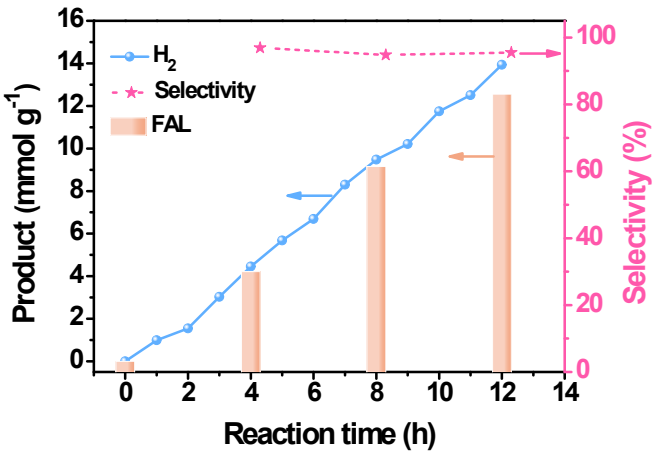

Figure S19. Photocatalytic activity of H_2 evolution coupled with FOL conversion over TC/CN in 40 mL of pure FOL.

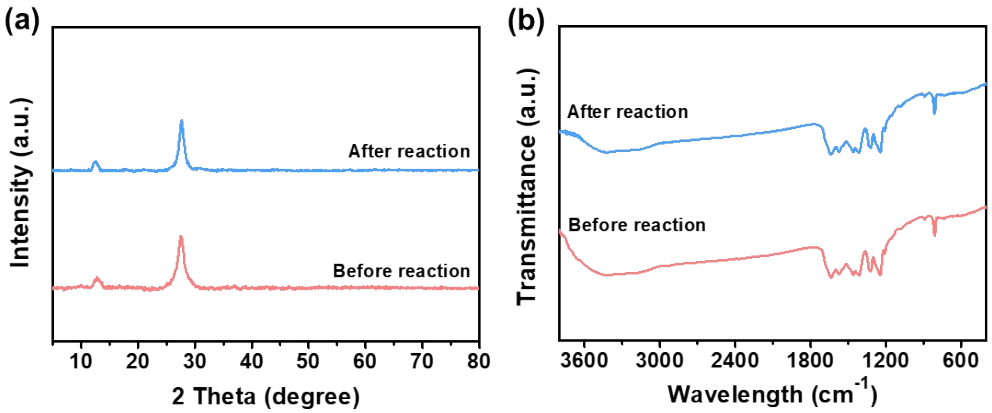

Figure S20. (a) XRD patterns and (b) FTIR spectra of TC/CN before and after the recycling tests.

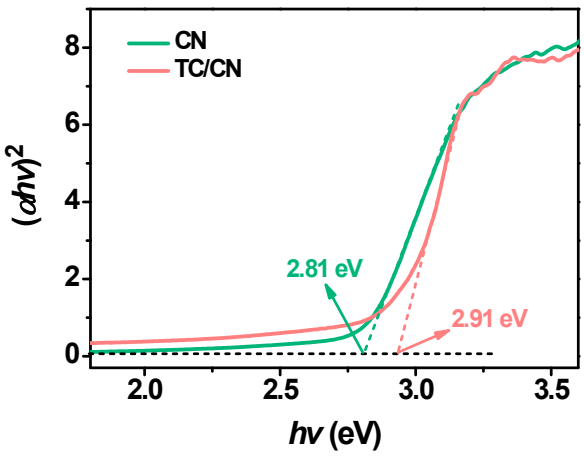

Figure S21. Tauc plots of CN and TC/CN.

Figure S21 shows the $(\alpha h\nu)^2$ as a function of photo energy (hν). Clearly, the E_g values of CN and TC/CN are estimated to be 2.81 and 2.91 eV, respectively, by extrapolating the plot to $(\alpha h\nu)^2 = 0$.

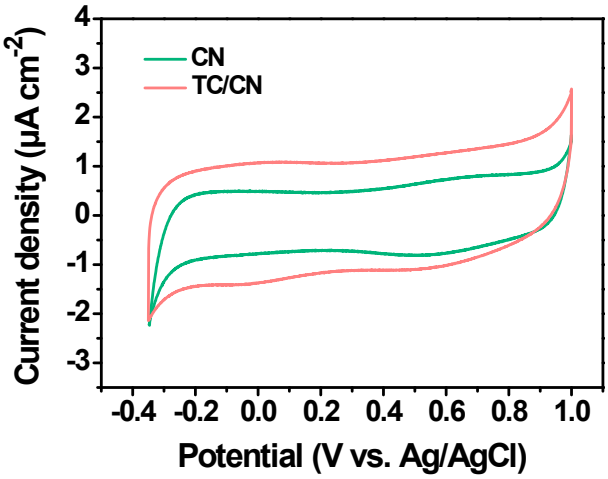

Figure S22. CV curves of CN and TC/CN.

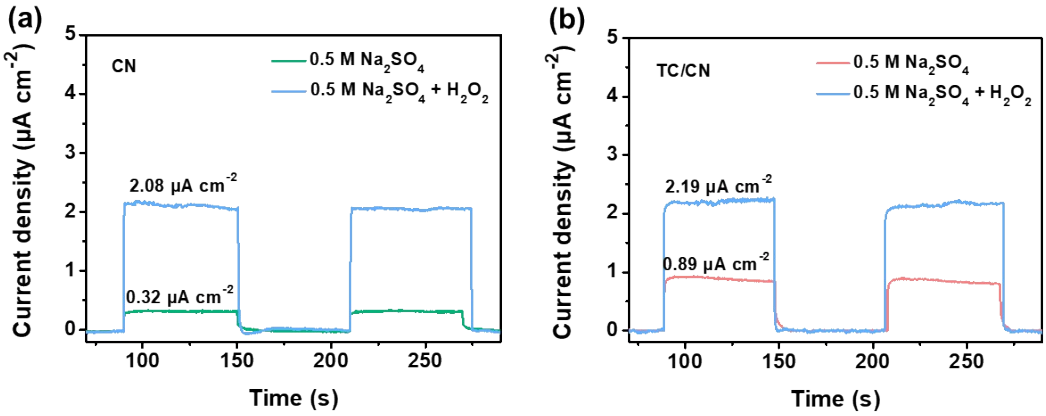

Figure S23. Transient *i-t* curves of (a) CN and (b) TC/CN measured in 0.5 M Na_2SO_4 and 0.5 M Na_2SO_4 + H_2O_2 solutions.

Employing H_2O_2 as a hole scavenger, the surface charge transfer efficiency (η_{trans}) can be determined by the following Equation[2,3]:

$$\eta_{trans} = J_{H_2O}/J_{H_2O_2} \tag{6}$$

where J_{H_2O} and $J_{H_2O_2}$ represent the photocurrent densities without and with the presence of H_2O_2,

respectively.

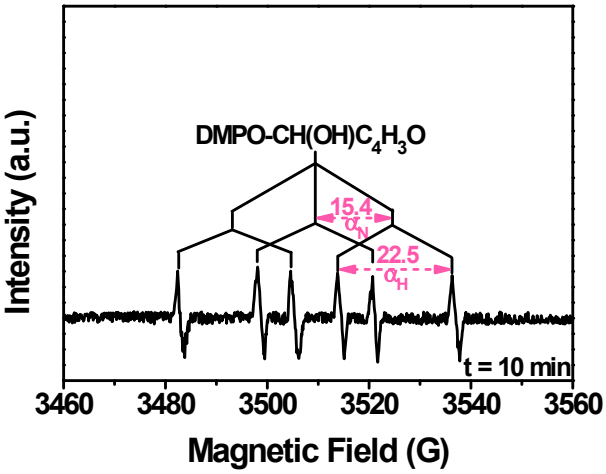

Figure S24. The quantitative analysis result of EPR spectrum of TC/CN with visible light irradiation for 10 min.

Figure S24 illustrates the clear observation of six distinct characteristic peaks at a g value of 2.0057 under light irradiation, the measured α_N = 15.4 and α_H = 22.5 correspond to the hyperfine splitting of nitrogen and hydrogen in nitroxide nitrogen, respectively. These findings align with previous research on DMPO-carbon radicals,[4-7] indicating the formation of •$CH(OH)C_4H_3O$ free radicals.

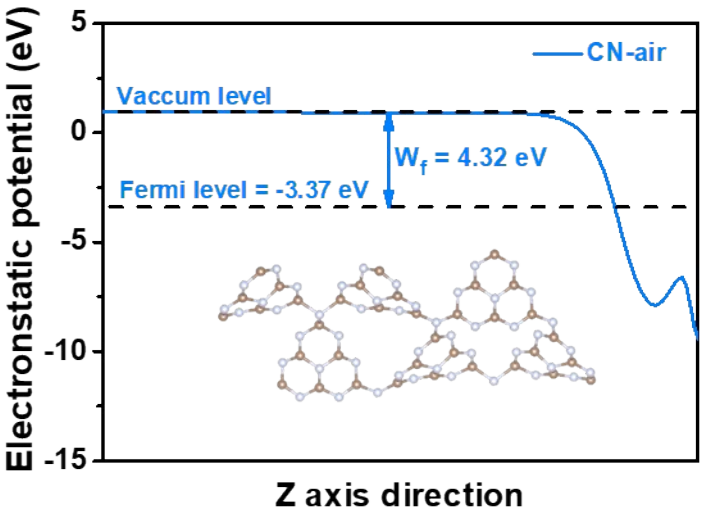

Figure S25. Calculated work functions and corresponding structural model of CN-air.

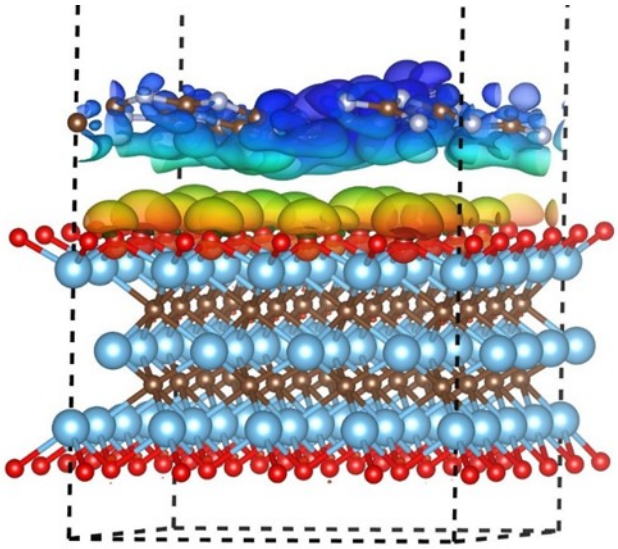

Figure S26. Calculated electrostatic potential at TC/CN interface.

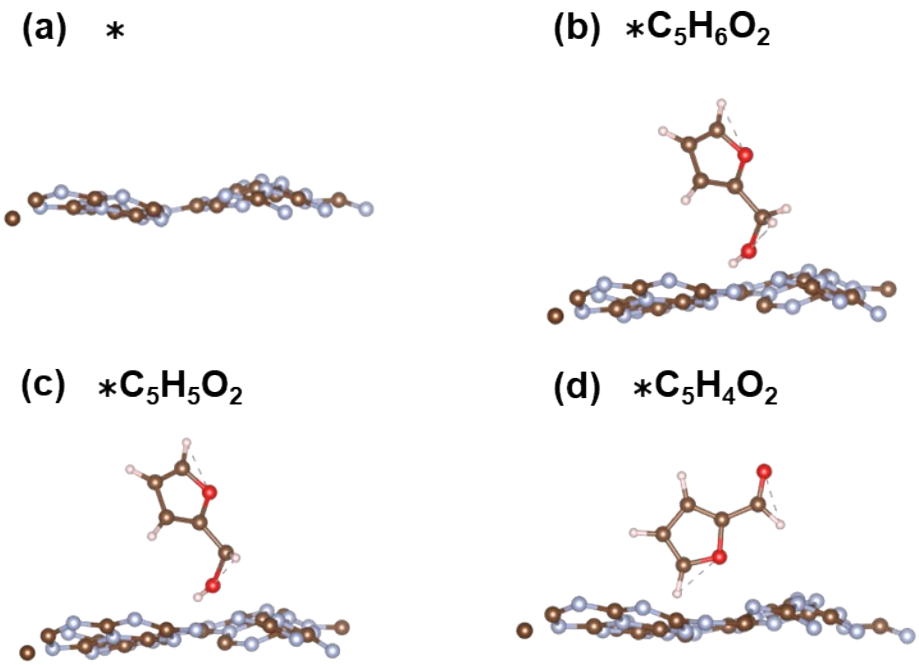

Figure S27. The optimized structures of the FOL oxidation processes (∗represents the surface of CN).

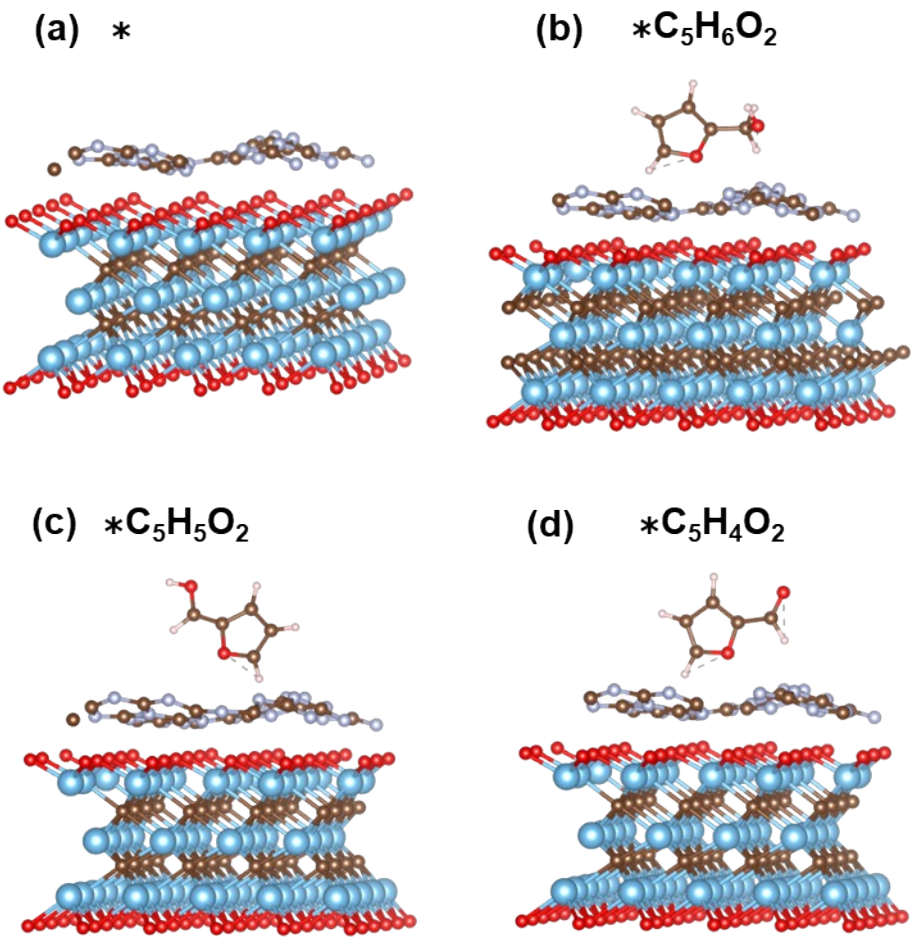

Figure S28. The optimized structures of the FOL oxidation processes (∗ represents the surface of TC/CN).

Supplementary Tables

Table S1. Summary of the mass content of TC, BET specific surface area, pore size and total pore volume values of CN, TC, and TC(*m*%)/CN samples.

Sample	TC content[a] (%)	BET Surface area (m^2 g^{-1})	Total pore volume (cm^3 g^{-1})	Average pore size (nm)
CN	0	119.3	0.65	19.6
TC	100	4.7	0.02	19.2
TC(2.5%)/CN	2.7	113.7	0.64	21.5
TC(3.5%)/CN	3.6	107.5	0.56	20.1
TC(5.3%)/CN	5.3	95.0	0.45	18.5
TC(7.5%)/CN	7.3	79.8	0.38	19.8
TC(9.1%)/CN	9.1	63.2	0.28	17.6

[a]the actual mass content of TC was determined from TGA analysis.

Table S2. Summary of the high-resolution XPS details of N 1s in the CN-air and CN.

Sample	Binding energy	Species	N/N_{total}	N_{2c}/N_{3c}	N (At%)	C (At%)	C/N
CN-air	398.4	C−N=C	0.60	2.97	58.4	43.1	0.74
	399.5	$N-(C)_3$	0.20				
	400.8	$C-N-H_x$	0.13				
CN	398.5	C−N=C	0.56	2.42	52.5	47.4	0.90
	399.5	$N-(C)_3$	0.23				
	400.9	$C-N-H_x$	0.10				

Notes: The values in the Table are obtained by calculating the percentage of peak area for the selected chemical bond relative to total peak area of the corresponding element, based on XPS analysis results.

Table S3. Composition of C, N, and H in CN-air and CN determined by elemental analysis and the calculated number of C and H atoms in a single formula unit.

Sample	N (wt%)	C (wt%)	H (wt%)	C/N Atomic ratio	C/H Atomic ratio	Number of N atoms	Number of H atoms
CN-air	60.28	34.41	1.52	0.666	1.886	27.027	9.544
CN	60.13	34.53	1.59	0.670	1.810	26.865	9.945

As shown in Table S3, the atomic ratio of C/N for CN is higher than that of CN-air, implying the existence of nitrogen vacancies in CN framework.

Table S4. Comparison of the photocatalytic activity for H_2 evolution and FOL oxidation over representative photocatalysts.

Photocatalyst	Reaction condition	H_2 evolution rate ($\mu mol\ g^{-1}\ h^{-1}$)	Liquid product and efficiency	Ref.
TC/CN	**300 W Xe lamp, 25 mg catalyst, 100 mL H_2O, 2 mM FOL**	**1165**	**FAL: 1220 $\mu mol\ g^{-1}\ h^{-1}$ Conv. (4 h): 57.6%**	**This work**
MoS_2-ZIS	300 W Xe lamp (>420 nm), 5 mg catalyst, 10 mL H_2O, 10 mM FOL, Ar	2938.7	FAL: 3043.8 $\mu mol\ g^{-1}\ h^{-1}$ Conv. (5 h): 65%	[4]
Ni-CdS	8 W blue LED (450 nm), 10 mg catalyst, 10 mL H_2O, 10 mM FOL, N_2	4051.3	FAL: 1470.5 $\mu mol\ g^{-1}\ h^{-1}$ Conv. (22 h): ~100%	[8]
$Ti_3C_2T_x$/CdS	300 W Xe lamp (>420 nm), 10 mg catalyst, 10 mL H_2O, 2.5 mM FOL, N_2	193.2	FAL: 194.2 $\mu mol\ g^{-1}\ h^{-1}$ Conv. (10 h): ~100%	[9]
$Ti_3C_2T_x$/CdS	3 W blue LED (420 nm), 10 mg catalyst, 4 mL H_2O, 25 mM FOL, N_2	609.2	FAL: 20.8 $\mu mol\ g^{-1}\ h^{-1}$ Conv. (12 h): 75.2%	[10]
Pt-ZnCdS	300 W Xe lamp, 25 mg catalyst, 40 mL H_2O, 1.4 mM FOL, N_2	1045	FAL: 1068.6 $\mu mol\ g^{-1}\ h^{-1}$ Conv. (3 h): 71%	[11]
$LaVO_4$/CN	300 W Xe lamp, 20 mg catalyst, 100 mL aqueous solution (10 mL FOL)	287	FAL: 238 $\mu mol\ g^{-1}\ h^{-1}$	[12]
Ni-Au/CN	300 W Xe lamp, 10 mg catalyst, 30 mL H_2O, 10 mM FOL, Ar	471.3	FAL: 206.2 $\mu mol\ g^{-1}\ h^{-1}$	[13]

Table S5. Controlled experimental results on photocatalytic FOL oxidation and H_2 evolution.

Entry	Photocatalyst	Solvent	Products (μmol)		Conversion (%)	Selectivity (%)	Yield (%)
			H_2	FAL			
1	TC/CN	DIW	116.5	122.0	57.6	97.2	56.0
2	–	DIW	0	0	0	0	0
3[a]	TC/CN	DIW	0	0	0	0	0
4	TC	DIW	0	0	0	0	0
5	TC/CN	CH_3CN	7.84	12.7	6.8	91.9	6.2
6[b]	TC/CN	CH_3CN	2.42	none	–	–	–

Light source: simulated solar light irradiation. Reaction solution: 100 mL of deionized water containing 0.2 mmol of FOL, 4 h. Catalyst: 25 mg. [a]without light irradiation; [b]CH_3CN was dried before use.

Table S6. Photocatalytic activity of TC/CN sample for H_2 evolution and selective oxidation of aromatic alcohols under simulated solar light irradiation.

Entry	Alcohol	H_2 (mmol g^{-1})	Oxidation product	Yield (mmol g^{-1})	Selectivity (%)
1	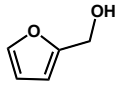	4.66	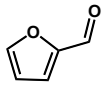	4.88	97.2%
2	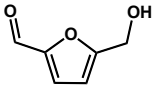	4.07	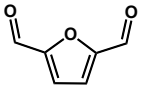	3.85	92.3%
3	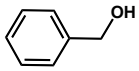	3.86	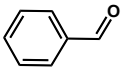	3.97	97.0%
4	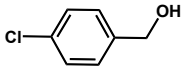	3.35	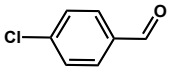	3.03	95.1%
5	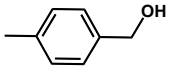	3.45	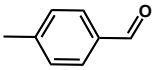	3.09	92.0%
6	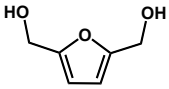	3.49	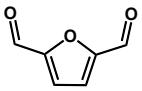	0.96	32.8%
7	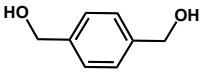	3.71	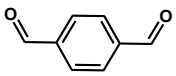	1.79	61.8%

Note: Reaction conditions: 25 mg of photocatalyst, 0.2 mmol of alcohol substrate, 100 mL of deionized water, simulated solar light, 4 h.

References

1. J. Zhang, E. Wang, S. Cui, S. Yang, X. Zou and Y. Gong, *Nano Lett.*, 2022, **22**, 1398-1405.
2. X. Chen, J. Wang, Y. Chai, Z. Zhang and Y. Zhu, *Adv. Mater.,* 2022, **33**, 2007479.
3. H. Zeng, Z. Li, G. Li, X. Cui, M. Jin, T. Xie, L. Liu, M. Jiang, X. Zhong, Y. Zhang, H. Zhang, K. Ba, Z. Yan, Y. Wang, S. Song, K. Huang and S. Feng, *Adv. Energy Mater.*, 2021, **12**, 2102765.
4. C.-L. Tan, M.-Y. Qi, Z.-R. Tang and Y.-J. Xu, *Appl. Catal. B: Environ.,* 2021, **298**, 120541.
5. S. Xie, Z. Shen, J. Deng, P. Guo, Q. Zhang, H. Zhang, C. Ma, Z. Jiang, J. Cheng, D. Deng and Y. Wang, *Nature Commun.*, 2018, **9**, 1181.
6. L. Jiao, D. Zhang, Z. Hao, F. Yu and X.-J. Lv, *ACS Catal.,* 2021, **11**, 8727-8735.
7. X. Peng, J. Li, L. Yi, X. Liu, J. Chen, P. Cai and Z. Wen, *Appl. Catal. B: Environ.,* 2022, **300**, 120737.
8. G. Han, Y.H. Jin, R.A. Burgess, N.E. Dickenson, X.M. Cao and Y. Sun, *J. Am. Chem. Soc.,* 2017, **139**, 15584-15587.
9. Y.-H. Li, F. Zhang, Y. Chen, J.-Y. Li and Y.-J. Xu, *Green Chem.,* 2020, **22**, 163-169.
10. J. Wang, X. Liu and Z. Li, *Chem. Asian. J.,* 2021, **16**, 2932-2938.
11. Z. Wang, L. Wang, B. Cheng, H. Yu and J. Yu, *Small methods,* 2021, **5**, 2100979.
12. X. Li, J. Hu, T. Yang, X. Yang, J. Qu and C.M. Li, *Nano Energy*, 2022, **92**, 106714.
13. Q. Yang, T. Wang, F. Han, Z. Zheng, B. Xing and B. Li, *J. Alloy. Compd.,* 2022, **897**, 163177.